JACS
JOURNAL OF THE AMERICAN CHEMICAL SOCIETY
pubs.acs.org/JACS
Article

Endowing Porphyrinic Metal–Organic Frameworks with High Stability by a Linker Desymmetrization Strategy

Wentao Han, Xing Ma, Jingxue Wang, Fucheng Leng, Chenfan Xie, and Hai-Long Jiang*

Cite This: J. Am. Chem. Soc. 2023, 145, 9665–9671
Read Online

ACCESS | Metrics & More | Article Recommendations | Supporting Information

ABSTRACT: The fabricating of metal–organic frameworks (MOFs) that integrate high stability and functionality remains a long-term pursuit yet a great challenge. Herein, we develop a linker desymmetrization strategy to construct highly stable porphyrinic MOFs, namely, USTC-9 (USTC represents the University of Science and Technology of China), presenting the same topological structure as the well-known PCN-600 that readily loses crystallinity in air or upon conventional activation. For USTC-9, the involved porphyrinic linker (TmCPP-M) with carboxylate groups located in the meta-position presents a chair-shaped conformation with lower C_{2h} symmetry than that (D_{4h}) of the common porphyrinic carboxylate (TCPP) linker in PCN-600. As a result, the wrinkled and interlocked linker arrangements collectively contribute to the remarkable stability of USTC-9. Given the high stability and porosity as well as Lewis acidity, USTC-9(Fe) demonstrates its excellent performance toward catalytic CO_2 cycloaddition with diverse epoxides at moderate temperature and atmospheric pressure.

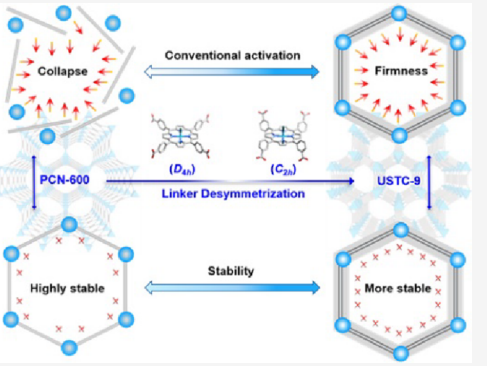

Downloaded via UNIV SCIENCE AND TECHNOLOGY CHINA on May 3, 2023 at 08:06:03 (UTC).
See https://pubs.acs.org/sharingguidelines for options on how to legitimately share published articles.

INTRODUCTION

Metal–organic frameworks (MOFs), as an important class of crystalline porous solid materials, have attracted great research interest in the past two decades due to their fascinating structures and potential applications.[1−4] Recently, the research endeavor on MOFs has gradually shifted from the construction of intriguing structures to functional applications,[5−11] posing high demands for their stability, functionality, high porosity, and structural tunability, among which porosity plays critical roles in diverse applications such as gas separation and storage, drug delivery, and catalysis.[12−15] In fact, since many MOFs are solvothermally synthesized in common solvents with high surface tension, such as *N*,*N*-dimethylformamide (DMF), dimethylsulfoxide (DMSO), *N*-methyl-2-pyrrolidone (NMP) or *N*,*N*-diethylformamide (DEF), these solvents residing in the MOF pores should be removed to release permanent porosity. This solvent removal (also called activation) process sometimes causes framework collapse of MOFs due to their limited stability. In addition to stability concerns during activation, the coordination bonds in MOFs are usually vulnerable to moisture or acidic or alkaline aqueous solutions, which is detrimental to their real-world applications.[16−18] To address this issue, different strategies have been developed to improve MOF stability, such as the incorporation of dangling hydrophobic groups,[19−21] creation of hydrophobic pore walls by post-synthetic modification,[22−24] hydrophobic surface treatment,[25−28] post-synthetic ion exchange,[29,30] composite material.[31,32] Although all these strategies are effective in improving MOF stability, unfortunately, in most cases, the intrinsic MOF porosity suffers from inevitable decreases to a certain degree due to the involvement of new components, which might give rise to compromised functionalities and properties. Moreover, some processes are complicated and not easy to be precisely controlled. In previous works, some low-symmetry linkers have been adopted in the synthesis of MOFs with novel topologies, which show the potential to produce stable MOFs.[33−36] In this context, the development of a facile approach to MOFs with high stability without introducing additional components or disturbing the intrinsic pore features is highly desired yet remains a significant challenge.

In addition to porosity, porphyrinic linkers with relatively large sizes are very promising for constructing functionalized and highly porous MOFs.[37−41] As a typical representative, the Fe-based porphyrinic MOF, namely, **PCN-600**, features a hexagonal structural topology (**stp**) and high chemical stability.[42] Moreover, multivariate MOFs can be fabricated based on the strong tunability of Fe_3O building blocks and metalloporphyrin linkers, making **PCN-600** an ideal platform MOF.[43] Unfortunately, the framework of **PCN-600** shows poor structural stability and collapses upon conventional

Received: January 26, 2023
Published: April 21, 2023

ACS Publications
© 2023 American Chemical Society

https://doi.org/10.1021/jacs.3c00957
J. Am. Chem. Soc. 2023, 145, 9665–9671

activation or even exposure to air due to the capillary forces caused by surface tension during the liquid−gas phase transition,[42,43] posing the challenge of generating permanent porosity. Accordingly, supercritical CO_2 activation, which generates very weak surface tension yet is not easily available, should be adopted as an alternative. This is an unfavorable restriction for its scale-up activation and further applications. To tackle this hurdle, it is necessary to carefully understand the geometries and symmetries of the framework structure, in which the 5,10,15,20-tetrakis(4-carboxyphenyl)porphine (TCPP) linker provides opportunities for improving stability.

In this work, a linker desymmetrization strategy was developed to synthesize isostructural Fe- and In-based porphyrinic MOFs, namely, **USTC-9**, in which the 5,10,15,20-tetrakis(*m*-carboxyphenyl)porphine (TmCPP) linker adopts lower C_{2h} symmetry than the D_{4h} symmetry of the TCPP linker in **PCN-600** (Figure 1). Interestingly, the

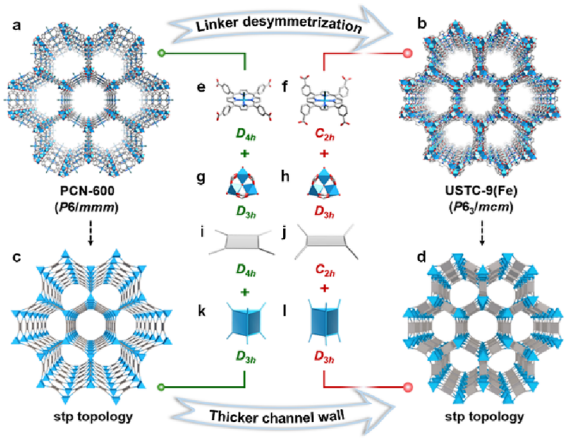

Figure 1. (a, c) Crystal structure and **stp** topology of **PCN-600**. (b, d) The crystal structure and **stp** topology of **USTC-9(Fe)**. (e, i) The four-connected, planar TCPP-Fe linker with D_{4h} symmetry in **PCN-600**. (f, j) The four-connected, chair-shaped TmCPP-Fe linker with C_{2h} symmetry in **USTC-9(Fe)**. (g, k) The six-connected Fe_3O cluster with D_{3h} symmetry in **PCN-600**. (h, l) The six-connected Fe_3O cluster with D_{3h} symmetry in **USTC-9(Fe)**. The FeO_6 polyhedra are shaded in cyan. Fe, C, O, N, and Cl are shown in cyan, gray, red, blue, and green, respectively. Hydrogen atoms are omitted for clarity.

TmCPP-M linkers adopt a wrinkled arrangement in the pore wall and interlocked permutation in the hexagonal ring, which creates the strong self-supporting ability of the skeleton and sheltered microenvironment around the vulnerable coordination bonds, thereby giving rise to much improved structural stability compared with isoreticular **PCN-600**. As a result, **USTC-9(Fe)** can not only present framework integrity upon conventional activation but also possess very high chemical stability, which features strong Lewis acidity and exhibits efficient conversion in the CO_2 cycloaddition with diverse epoxides.

RESULTS AND DISCUSSION

Modulator-assisted synthesis has been proven to be a skillful and powerful strategy in the controlled growth of porphyrinic MOF crystals.[42,43] Unfortunately, when a single modulator was employed in the synthesis of **USTC-9(Fe)**, only powdery samples or very tiny crystals can be obtained. To our delight, the solvothermal reaction of H_2TmCPP and $FeCl_3{\cdot}6H_2O$ at 160 °C with a dual modulator (trifluoroacetic acid and nitric acid) strategy was demonstrated to be effective in the control of nucleation and growth, yielding single crystals of **USTC-9(Fe)**. Furthermore, the $Fe_2Mn(\mu_3\text{-}O)(CH_3COO)_6$ cluster can also work as a starting material to synthesize **USTC-9(Fe_2Mn)** through a similar recipe (Figure S1). Notably, single crystals of **USTC-9(In)** can be synthesized with a different recipe by the solvothermal reaction of H_2TmCPP and $In(OH)_3$ with nitric acid as a single modulator in DMF at 120 °C. Both **USTC-9(Fe)** and **USTC-9(In)** possess a similar rod morphology (Figure S2).

Single-crystal X-ray diffraction analysis indicates that **USTC-9(Fe)** and **USTC-9(In)** are isostructural and crystallize in the hexagonal system with a space group of $P6_3/mcm$ (Table S1). Therefore, **USTC-9(Fe)** is taken as an example to illustrate their crystal structures. There are two crystallographically unique Fe(III) ions in the structure (Figure S3a), of which Fe1 is pseudo-octahedrally coordinated by four oxygen atoms from four linkers in the basal plane as well as one oxygen atom from the μ_3-O group and one terminal oxygen atom in the axial direction, and Fe2 is coordinated by four nitrogen atoms coming from one porphyrin ring and a chlorine atom at the axial position (Figure S3a). **USTC-9** exhibits a three-dimensional (3D) extended network in **stp** topology with hexagonal 1D channels 17.28 × 13.50 $Å^2$ in size (Figure S3b,c). The hexagonal 1D channels, which consist of six-connected M_3O clusters and four-connected TmCPP-M (M = Fe or In) linkers (Figure S4a), are periodically arranged in a honeycomb-like network (Figure 2a). Each carboxylate group on the TmCPP-M linker is connected with one M_3O cluster in a bidentate coordination mode (Figure S4a).

It is worth noting that, although **USTC-9** possesses a framework topology (**stp**) and chemical composition similar to those reported for **PCN-600**, the structural details originating from the unique TmCPP-M linker are distinctly different (Figure 2). Specifically, TmCPP-M with carboxylate groups located in the meta-position relative to the central conjugate

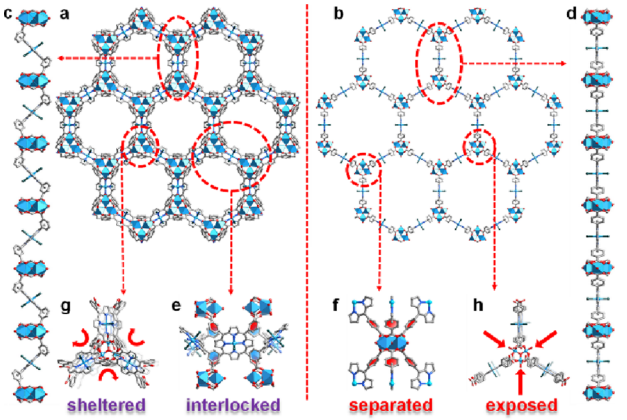

Figure 2. (a) **USTC-9(Fe)** with thick channel walls. (b) **PCN-600** with thin channel walls. (c) The wrinkled arrangement of chair-shaped TmCPP-Fe linkers. (d) The flat arrangement of planar TCPP-Fe linkers. (e) The interlocked arrangement of TmCPP-M linkers. The two types of benzene rings that are locked with each other are marked by red and blue, respectively. (f) The separated arrangement of TCPP-Fe linkers. Six benzene rings linked to the same cluster are marked in red. (g) The six-connected M_3O cluster in **USTC-9** with coordination bonds sheltered in the thickened channel wall. (h) The six-connected Fe_3O cluster in **PCN-600** with coordination bonds exposed to the hexagonal channel.

https://doi.org/10.1021/jacs.3c00957
J. Am. Chem. Soc. 2023, 145, 9665−9671

ring is deformed from planarity in particular conformations to optimize the coordination bonds and adapt to the final framework structure.[44] In **USTC-9**, the carboxyphenyl groups of the TmCPP-M linker are distributed on the upper and lower sides of the central conjugate ring, which contributes to the constrictive chair-shaped linker conformation in C_{2h} symmetry (Figure 1f,j). The chair-shaped TmCPP-M linkers adopt wrinkled arrangements interconnected by the M_3O clusters into the 1D chain (Figure 2c), which induces partial benzene rings to locate on the inner walls of the channels, leading to thickened channel walls compared with those in **PCN-600** (Figure 2a,b). More interestingly, the TmCPP-M linkers adopt the interlocked form to make their benzene rings lock with each other (Figure 2e, Figure S5). With the above connection ways, the coordination bonds in **USTC-9** are sheltered into the interior of the channel walls (Figure 2g). In comparison, the planar TCPP-Fe linkers in D_{4h} symmetry (Figure 1e,i) adopt the flat arrangement in the 1D channel of **PCN-600** (Figure 2d) and interconnect in the separated form by the Fe_3O clusters (Figure 2f), resulting in the thin channel wall with the coordination bonds being exposed and vulnerable (Figure 2f,h).

The above structural features account for the high stability of **USTC-9**. To our delight, unlike the strict supercritical CO_2 activation required for **PCN-600**, **USTC-9** can be activated through a conventional activation process, i.e., solvent exchange followed by simple heating and vacuum treatments (Figure 3a and Figure S6). N_2 sorption isotherms of **USTC-9(Fe)** and **USTC-9(In)** show typical type I microporous isotherms with Brunauer–Emmett–Teller (BET) surface areas of 2294 and 2067 m^2/g, respectively (Figures S7 and S8). The corresponding pore size distributions based on density functional theory (DFT) analysis are consistent with the structural data, suggesting that the framework structures can be well maintained after conventional activation. Moreover, the crystallinity of **USTC-9(Fe)** remains unchanged upon exposure to ambient atmosphere for at least 1 month (Figure 3a), which is of great importance for common preservation and subsequent applications. In sharp contrast, the crystallinity of **PCN-600** completely disappears after conventional activation (Figure S9)[42] and rapidly decreases after losing DMF solvent in the channels upon exposure to air (Figure 3c), indicating that its structure is vulnerable to surface tension during the liquid–gas phase transition.

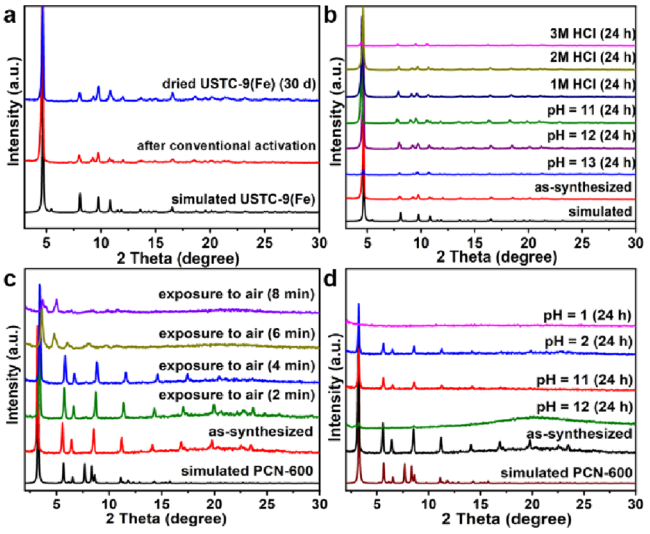

Figure 3. (a, c) Powder X-ray diffraction (XRD) patterns of (a) **USTC-9(Fe)** and (c) **PCN-600** after exposure to air for different times. (b, d) Powder XRD patterns of (b) **USTC-9(Fe)** and (d) **PCN-600** after soaking in water and acid and base aqueous solutions for 24 h.

To investigate the chemical stability of **USTC-9(Fe)**, it was immersed in aqueous acidic and alkaline solutions as well as a variety of organic solvents for 24 h. It was demonstrated to be stable from 2 M HCl to pH = 12 aqueous solutions (Figure 3b, Figure S10a). The upper solutions turned dark green in 3 M HCl and dark red in pH = 13 aqueous solutions, inferring the color of the soluble porphyrin linker, which implies the collapsed MOF skeleton (Figure S11a). Moreover, the supernatant remained colorless in different organic solvents (Figure S11b), suggesting the high stability of **USTC-9(Fe)** in these solvents. Powder XRD patterns and N_2 sorption isotherms unambiguously indicated that the crystallinity and framework integrity of **USTC-9(Fe)** can be well maintained under the abovementioned conditions (Figure 3a,b, Figure S12). In contrast, the structure of **PCN-600** can be maintained in solutions with pH values from 2 to 11 and some organic solvents; its crystallinity is completely lost in solutions with pH = 1 and 12 (Figure 3d, Figure S13). Apparently, the chemical stability of **USTC-9(Fe)** is significantly improved compared with that of **PCN-600** (Figure 3).[42] Meanwhile, the high chemical stability of **USTC-9(Fe)** surpasses that of many other iron-based carboxylate MOFs (Figure S14).[45−49] Notably, given the difference in the M–O coordination bond strength originating from different metal centers, the stability of **USTC-9(In)** is slightly lower than that of **USTC-9(Fe)**. The framework of **USTC-9(In)** remains intact in different organic solvents and pH = 2–11 aqueous solutions for 24 h (Figures S15 and S16), which is also excellent in the reported indium-based MOFs (Figure S17).[50] In addition, thermogravimetric (TG) analyses indicate that both **USTC-9(Fe)** and **USTC-9(In)** all exhibit high thermal stability and the frameworks can be maintained up to 330 °C (Figure S18).

The reasons behind the obviously improved stability of **USTC-9** built by TmCPP-M with C_{2h} symmetry can be unveiled from its structural details. Compared to **PCN-600**, the chair configuration of the TmCPP-M linker gives rise to the closer linker arrangement and thickened channel walls, which help to minimize the free energy and benefits structure stability.[51] Furthermore, six TmCPP-M linkers in the hexagonal ring adopt the wise interlocked connecting way and their benzene rings support each other, which is of great importance to afford a robust structure and resist capillary forces during the conventional activation. In addition, with the rotation of metal nodes, the coordination bonds point inside the channel wall and locate in a sheltered microenvironment so that they can be protected by thickened channel walls and thereby will enhance the chemical stability. All of the above factors work together and contribute to the high stability of **USTC-9**, although it has the same framework topology and very similar composition and structure to those of **PCN-600**. With high stability and permanent porosity by facile conventional activation, **USTC-9** with functionalized porphyrin units and high tailorability would provide great opportunities for diverse applications.

Encouraged by the above results, the abundant metal sites in **USTC-9** afford well-accessible Lewis acidic sites and inspire us

https://doi.org/10.1021/jacs.3c00957
J. Am. Chem. Soc. 2023, 145, 9665–9671

to investigate their catalytic performance. As one of the CO_2 utilization ways by converting it into valuable chemical products, CO_2 cycloaddition with epoxides is one of the most promising strategies to meet the challenge of excess CO_2 emissions in the atmosphere.[52−55] Due to the release of the ring-strain energy in epoxides, the reaction can be promoted by highly active catalysts under mild conditions. With this in mind, the conversion of CO_2 cycloaddition with different epoxides to cyclic carbonates has been investigated by using **USTC-9** in the presence of tetrabutylammonium bromide (TBAB), serving as a nucleophile (Figure S19). Delightedly, **USTC-9(Fe)** is demonstrated to be an excellent catalyst in the catalytic conversion of epibromohydrin and possesses very high efficiency with a conversion of 96.4% (Figure 4a),

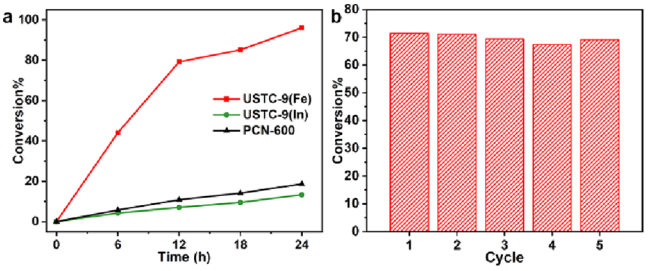

Figure 4. (a) Catalytic conversion of CO_2 cycloaddition with epibromohydrin over different catalysts in 24 h. (b) Recycling catalytic performance of the CO_2 cycloaddition of epibromohydrin over **USTC-9(Fe)** (12 h for each cycle).

possibly due to the strong Lewis acidity and CO_2 adsorption ability of **USTC-9(Fe)** (Figure S20). Unexpectedly, the significant activity difference between **USTC-9(In)** and **USTC-9(Fe)** can be observed (Figure 4a, Table S2). The acidity strength is examined by NH_3 temperature-programmed desorption (TPD).[56,57] Broad desorption peaks can be observed in the range of 50−250 °C, which is ascribed to the adsorption of NH_3 on the Lewis acid sites. The Lewis acid strength of **USTC-9(Fe)** is evaluated by the temperature of the maximum NH_3 desorption peak (126.2 °C), which is higher than that (105.7 °C) of **USTC-9(In)**, accounting for the superior catalytic activity of **USTC-9(Fe)** (Figure S21). In addition, **USTC-9(Fe)** exhibits excellent catalytic recyclability in the CO_2 cycloaddition with epibromohydrin due to its high stability (Figure 4b, Figure S22a). In contrast, although **PCN-600** presents a certain conversion at the early stage of the reaction, the poor stability gives rise to the rapid disappearance of its crystallinity. The site accessibility of **PCN-600** decreases due to the collapse of the pore, which explains its less activity than the $Fe_3O(OOCCH_3)_6$ cluster (Figure S22b, Table S2).

Under the optimized conditions, a wide range of epoxides has been examined in the catalytic reaction with **USTC-9(Fe)** (Table 1). To our delight, good to excellent conversions and high selectivity can be obtained for diverse substrates with electron-withdrawing or -donating groups, at 70 °C and 1 atm of CO_2, which reflects the good tolerance of **USTC-9(Fe)** to different substrates.

CONCLUSIONS

In summary, the highly stable MOFs, **USTC-9(M)** (M = Fe, In), have been successfully constructed by a linker desymmetrization strategy. **USTC-9(Fe)** presents the same framework topology and very similar chemical composition as **PCN-600**.

Table 1. CO_2 Cycloaddition with Diverse Epoxides Catalyzed by USTC-9(Fe)[a]

Entry	Substrate	Time / day	Conversion / %[b]	Selectivity / %[b]
1		1	95.1	>99
2		1	96.4	>99
3		1	73.0	>99
4		2	87.8	83.4
5	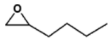	1	60.6	90.1
6		1	86.3	>99

[a]Reaction conditions: 0.1 mmol substrate, 10 mg of catalyst, 10 mg of TBAB, 3 mL acetonitrile, 1 atm CO_2, 70 °C. [b]Determined by gas chromatography and mass spectrum, the by-product might be corresponding diols, aldehydes, ketones, or some oxidation products.

In comparison to TCPP-Fe with D_{4h} symmetry in **PCN-600**, the unique arrangements of the TmCPP-Fe linker with C_{2h} symmetry in **USTC-9(Fe)** significantly increase the structural firmness and tolerance to capillary forces, which result in much enhanced chemical stability not only in the aqueous solutions ranging from 2 M HCl to pH = 12 and diverse solvents but also in air for over 1 month, among the best of all reported Fe carboxylate MOFs. Given the remarkable stability, high porosity, and Lewis acidity, **USTC-9(Fe)** exhibits excellent catalytic performance in the CO_2 cycloaddition with epoxides under mild conditions. This work develops a novel solution to improve the stability of MOFs by linker desymmetrization and microenvironment modulation of coordination bonds, which not only leads to the creation of a new platform MOF, **USTC-9**, but also increases the understanding of MOF stability. This work provides a novel strategy and opens a new avenue to the development of functionalized MOFs with enhanced chemical stability, which is of significance for future MOF applications.

MATERIALS AND METHODS

Materials and Equipment. All chemicals were obtained from commercial sources and used without further purification unless otherwise mentioned. Deionized water with a specific resistance of 18.25 MΩ·cm was obtained by reverse osmosis followed by ion exchange and filtration (Cleaned Water Treatment Co., Ltd., Hefei). Powder X-ray diffraction (XRD) patterns were obtained on a Japan Rigaku SmartLab™ rotation anode X-ray diffractometer (MiniFlex 600) equipped with graphite-monochromated Cu Kα radiation (λ = 1.54178 Å). Nitrogen sorption isotherms were measured by using automatic volumetric adsorption equipment (Micromeritics ASAP 2020). Thermogravimetric analysis (TGA) was performed on a TGA Q5000 integration thermal analyzer at a heating rate of 10 °C min^{-1} under an air atmosphere. The contents of Fe and Mn were measured by inductively coupled plasma atomic emission spectroscopy (ICP-AES, Optima 7300 DV). Field-emission scanning electron microscopy (FE-SEM) was carried out with a field emission scanning electron microanalyzer (Zeiss Supra 40 scanning electron microscopies at an acceleration voltage of 5 kV). Temperature-programmed desorption of ammonia (NH_3-TPD) was conducted on an AutoChem II 2920 adsorption instrument. The catalytic reaction products were analyzed and identified by gas chromatography (GC, Shimadzu 2010 Plus with a 0.25 mm × 30 m Rtx-5 capillary column) and further determined by an Agilent Technologies 7890A GC with a detector of an Agilent

https://doi.org/10.1021/jacs.3c00957
J. Am. Chem. Soc. 2023, 145, 9665−9671

Technologies 5975C mass spectrometer. Elemental analysis (EA) was performed with a vario EL III analyzer.

Preparation of USTC-9(Fe). Typically, DMF (2 mL), HNO_3 (150 μL), and TFA (140 μL) were added in sequence into a glass vial with $FeCl_3 \cdot 6H_2O$ (12 mg, 0.044 mmol) and H_2TmCPP (5 mg, 0.006 mmol). Then, the glass vial was sonicated until the ingredients were completely resolved and was then placed in a preheated oven at 160 °C for 10 h. After cooling to room temperature, dark-purple rod-shaped crystals were obtained (5.7 mg, 87%). Anal. calcd. For **USTC-9(Fe)**: C, 55.94; H, 2.35; N, 5.44%. Found: C, 56.07; H, 2.06; N, 5.53%.

Preparation of USTC-9(In). Typically, DMF (2 mL) and HNO_3 (300 μL) were added in sequence into a glass vial with $In(OH)_3$ (10 mg, 0.060 mmol) and H_2TmCPP (10 mg, 0.013 mmol). Then, the glass vial was sonicated until the linker was completely resolved and was then placed in the preheated oven at 120 °C for 2 days. After cooling to room temperature, purple rod-shaped crystals were obtained (6.2 mg, 48%). Anal. calcd. For **USTC-9(In)**: C, 47.89; H, 2.01; N, 4.65%. Found: C, 48.02; H, 2.31; N, 4.71%.

Preparation of PCN-600. The synthesis method followed the previous report with some modifications.[42] Typically, DMF (8 mL) and TFA (1.2 mL) were sequentially added into a Teflon reactor with the $Fe_3O(OOCCH_3)_6$ cluster (40 mg, 0.068 mmol) and TCPP-Fe (40 mg, 0.047 mmol). Then, the reactor was sonicated until the linker was completely dissolved and was then placed in a preheated oven at 150 °C for 12 h. After cooling down to room temperature, purple rod-shaped **PCN-600** crystals were obtained by careful washing and supercritical CO_2 drying.

Sample Activation and N_2 Adsorption Measurements. The as-synthesized **USTC-9** (~50 mg) sample was washed with DMF five times to remove unreacted precursors and then solvent-exchanged with acetone five times within 2 days. The sample was typically activated at 165 °C under vacuum for 12 h. Prior to the adsorption measurement, the sample was dried through the degas function of the adsorption instrument for 12 h at 140 °C.

Catalytic CO_2 Cycloaddition with Epoxides. In a typical experiment, a mixture of catalyst (10 mg), epoxides (0.1 mmol), MeCN (3 mL), and TBAB (10 mg) was added into a 10 mL round-bottom flask, which was connected to a CO_2 balloon. Then, the mixture was stirred at 70 °C for 24 h. Upon completion of the reaction, 100 μL of the resultant supernatant was taken into a solvent of MeCN (400 μL) and then the yield of the product was detected by GC. For the catalytic recycling experiments, the reaction time for each cycle was 12 h. The catalyst was separated by centrifugation after the reaction and thoroughly washed with 5 mL MeCN and 5 mL acetone three times. Then, it was dried in vacuum for 6 h for the next run.

X-ray Crystallography. Suitable single crystals of **USTC-9** were selected and mounted onto the matched nylon ring using Fomblin oil. The single-crystal X-ray diffraction data for the **USTC-9** series were collected using the synchrotron radiation X-ray source at 173 K, λ = 0.65250 Å, at the Shanghai Synchrotron Radiation Facility. Determinations of the crystal system, cell dimensions, and orientation matrix were performed according to established procedures. Crystal structures were solved by direct methods and refined by full-matrix least-squares methods against F^2 using the SHELXL-97 program package as well as Olex2 software.[58,59] Subsequent difference Fourier synthesis and least-square refinement revealed the positions of the remaining non-hydrogen atoms. The non-hydrogen atoms were refined with anisotropic displacement parameters, while the hydrogens were fixed at calculated positions and refined isotropically. The solvent molecules are highly disordered and hard to refine by using conventional discrete-atom models. Hence, the contribution of solvent molecules was removed by the SQUEEZE routine in PLATON.[60] The crystallographic data and structure refinement for **USTC-9** are summarized in Table S1. These data have been deposited at the Cambridge Crystallographic Data Centre via www.ccdc.cam.ac.uk with codes 2064545 and 2064546 and can be obtained free of charge.

■ ASSOCIATED CONTENT

Supporting Information

The Supporting Information is available free of charge at https://pubs.acs.org/doi/10.1021/jacs.3c00957.

Details on linker preparation, characterization data, and figures (PDF)

Accession Codes

CCDC 2064545−2064546 contain the supplementary crystallographic data for this paper. These data can be obtained free of charge via www.ccdc.cam.ac.uk/data_request/cif, or by emailing data_request@ccdc.cam.ac.uk, or by contacting The Cambridge Crystallographic Data Centre, 12 Union Road, Cambridge CB2 1EZ, UK; fax: +44 1223 336033.

■ AUTHOR INFORMATION

Corresponding Author

Hai-Long Jiang − *Hefei National Research Center for Physical Sciences at the Microscale, Department of Chemistry, University of Science and Technology of China, Hefei, Anhui 230026, P. R. China;* orcid.org/0000-0002-2975-7977; Email: jianglab@ustc.edu.cn

Authors

Wentao Han − *Hefei National Research Center for Physical Sciences at the Microscale, Department of Chemistry, University of Science and Technology of China, Hefei, Anhui 230026, P. R. China*

Xing Ma − *Hefei National Research Center for Physical Sciences at the Microscale, Department of Chemistry, University of Science and Technology of China, Hefei, Anhui 230026, P. R. China*

Jingxue Wang − *Hefei National Research Center for Physical Sciences at the Microscale, Department of Chemistry, University of Science and Technology of China, Hefei, Anhui 230026, P. R. China*

Fucheng Leng − *Hefei National Research Center for Physical Sciences at the Microscale, Department of Chemistry, University of Science and Technology of China, Hefei, Anhui 230026, P. R. China*

Chenfan Xie − *Hefei National Research Center for Physical Sciences at the Microscale, Department of Chemistry, University of Science and Technology of China, Hefei, Anhui 230026, P. R. China*

Complete contact information is available at: https://pubs.acs.org/10.1021/jacs.3c00957

Author Contributions

All authors have given approval to the final version of the manuscript.

Notes

The authors declare no competing financial interest.

■ ACKNOWLEDGMENTS

This work was supported by the National Key Research and Development Program of China (2021YFA1500400), the Strategic Priority Research Program of the CAS (XDB0450302), the National Natural Science Foundation of China (U22A20401, 22161142001), and Fundamental Research Funds for the Central Universities (WK3450000007).

REFERENCES

(1) Furukawa, H.; Cordova, K. E.; O'Keeffe, M.; Yaghi, O. M. The Chemistry and applications of metal-organic frameworks. *Science* **2013**, *341*, 1230444.

(2) Zhou, H.-C.; Kitagawa, S. Metal-organic frameworks (MOFs). *Chem. Soc. Rev.* **2014**, *43*, 5415−5418.

(3) Islamoglu, T.; Goswami, S.; Li, Z.; Howarth, A. J.; Farha, O. K.; Hupp, J. T. Postsynthetic tuning of metal-organic frameworks for targeted applications. *Acc. Chem. Res.* **2017**, *50*, 805−813.

(4) Jeoung, S.; Kim, S.; Kim, M.; Moon, H. R. Pore engineering of metal-organic frameworks with coordinating functionalities. *Coord. Chem. Rev.* **2020**, *420*, 213377.

(5) Li, B.; Wen, H.-M.; Cui, Y.; Zhou, W.; Qian, G.; Chen, B. Emerging multifunctional metal-organic framework materials. *Adv. Mater.* **2016**, *28*, 8819−8860.

(6) Zhu, B.; Zou, R.; Xu, Q. Metal-organic framework based catalysts for hydrogen evolution. *Adv. Energy Mater.* **2018**, *8*, 1801193.

(7) Ding, M.; Flaig, R. W.; Jiang, H.-L.; Yaghi, O. M. Carbon capture and conversion using metal-organic frameworks and MOF-based materials. *Chem. Soc. Rev.* **2019**, *48*, 2783−2828.

(8) Wang, H.-N.; Zou, Y.-H.; Sun, H.-X.; Chen, Y.; Li, S.-L.; Lan, Y.-Q. Recent progress and perspectives in heterogeneous photocatalytic CO_2 reduction through a solid-gas mode. *Coord. Chem. Rev.* **2021**, *438*, 213906.

(9) Pang, Q.; Yang, L.; Li, Q. Vacancies in metal-organic frameworks: Formation, arrangement, and functions. *Small Struct.* **2022**, *3*, 2270016.

(10) Huang, N.-Y.; Shen, J.-Q.; Zhang, X.-W.; Liao, P.-Q.; Zhang, J.-P.; Chen, X.-M. Coupling ruthenium bipyridyl and cobalt imidazolate units in a metal-organic framework for an efficient photosynthetic overall reaction in diluted CO_2. *J. Am. Chem. Soc.* **2022**, *144*, 8676−8682.

(11) Xiao, J.-D.; Jiang, H.-L. Metal-organic frameworks for photocatalysis and photothermal catalysis. *Acc. Chem. Res.* **2019**, *52*, 356−366.

(12) Lin, R.-B.; Zhang, Z.; Chen, B. Achieving high performance metal-organic framework materials through pore engineering. *Acc. Chem. Res.* **2021**, *54*, 3362−3376.

(13) Ma, J.; Kalenak, A. P.; Wong-Foy, A. G.; Matzger, A. J. Rapid guest exchange and ultra-low surface tension solvents optimize metal-organic framework activation. *Angew. Chem., Int. Ed.* **2017**, *56*, 14618−14621.

(14) Hong, A. N.; Yang, H.; Bu, X.; Feng, P. Pore space partition of metal-organic frameworks for gas storage and separation. *EnergyChem* **2022**, *4*, 100080.

(15) Mondloch, J. E.; Katz, M. J.; Planas, N.; Semrouni, D.; Gagliardi, L.; Hupp, J. T.; Farha, O. K. Are Zr_6-based MOFs water stable? Linker hydrolysis vs. capillary-force-driven channel collapse. *Chem. Commun.* **2014**, *50*, 8944−8946.

(16) Healy, C.; Patil, K. M.; Wilson, B. H.; Hermanspahn, L.; Harvey-Reid, N. C.; Howard, B. I.; Kleinjan, C.; Kolien, J.; Payet, F.; Telfer, S. G.; Kruger, P. E.; Bennett, T. D. The thermal stability of metal-organic frameworks. *Coord. Chem. Rev.* **2020**, *419*, No. 213388.

(17) Yuan, S.; Feng, L.; Wang, K.; Pang, J.; Bosch, M.; Lollar, C.; Sun, Y.; Qin, J.; Yang, X.; Zhang, P.; Wang, Q.; Zou, L.; Zhang, Y.; Zhang, L.; Fang, Y.; Li, J.; Zhou, H.-C. Stable metal-organic frameworks: Design, synthesis, and applications. *Adv. Mater.* **2018**, *30*, 1704303.

(18) Ding, M.; Cai, X.; Jiang, H.-L. Improving MOF stability: approaches and applications. *Chem. Sci.* **2019**, *10*, 10209−10230.

(19) Gong, W.; Xie, H.; Idrees, K. B.; Son, F. A.; Chen, Z.; Sha, F.; Liu, Y.; Cui, Y.; Farha, O. K. Water sorption evolution enabled by reticular construction of Zirconium metal-organic frameworks based on a unique [2.2]paracyclophane scaffold. *J. Am. Chem. Soc.* **2022**, *144*, 1826−1834.

(20) Jiang, Z.-R.; Ge, J.; Zhou, Y.-X.; Wang, Z. U.; Chen, D.; Yu, S.-H.; Jiang, H.-L. Coating sponge with a hydrophobic porous coordination polymer containing a low-energy CF_3-decorated surface for continuous pumping recovery of an oil spill from water. *NPG Asia Mater.* **2016**, *8*, No. e253.

(21) Zhu, N.-X.; Wei, Z.-W.; Chen, C.-X.; Xiong, X.-H.; Xiong, Y.-Y.; Zeng, Z.; Wang, W.; Jiang, J.-J.; Fan, Y.-N.; Su, C.-Y. High water adsorption MOFs with optimized pore-nanospaces for autonomous indoor humidity control and pollutants removal. *Angew. Chem., Int. Ed.* **2022**, *61*, No. e202112097.

(22) Nguyen, J. G.; Cohen, S. M. Moisture-resistant and superhydrophobic metal−organic frameworks obtained via postsynthetic modification. *J. Am. Chem. Soc.* **2010**, *132*, 4560−4561.

(23) Li, L.; Li, Z.; Yang, W.; Huang, Y.; Huang, G.; Guan, Q.; Dong, Y.; Lu, J.; Yu, S.-H.; Jiang, H.-L. Integration of Pd nanoparticles with engineered pore walls in MOFs for enhanced catalysis. *Chem* **2021**, *7*, 686−698.

(24) Sun, D.; Adiyala, P. R.; Yim, S.-J.; Kim, D.-P. Pore-surface engineering by decorating metal-oxo nodes with phenylsilane to give versatile super-hydrophobic metal-organic frameworks (MOFs). *Angew. Chem., Int. Ed.* **2019**, *58*, 7405−7409.

(25) Zhang, W.; Hu, Y.; Ge, J.; Jiang, H.-L.; Yu, S.-H. A facile and general coating approach to moisture/water-resistant metal-organic frameworks with intact porosity. *J. Am. Chem. Soc.* **2014**, *136*, 16978−16981.

(26) Yang, S.; Peng, L.; Sun, D. T.; Asgari, M.; Oveisi, E.; Trukhina, O.; Bulut, S.; Jamali, A.; Queen, W. L. A new post-synthetic polymerization strategy makes metal-organic frameworks more stable. *Chem. Sci.* **2019**, *10*, 4542−4549.

(27) Ding, M.; Jiang, H.-L. Improving water stability of metal-organic frameworks by a general surface hydrophobic polymerization. *CCS Chem.* **2021**, *3*, 2740−2748.

(28) Sun, Q.; He, H.; Gao, W.-Y.; Aguila, B.; Wojtas, L.; Dai, Z.; Li, J.; Chen, Y.-S.; Xiao, F.-S.; Ma, S. Imparting amphiphobicity on single-crystalline porous materials. *Nat. Commun.* **2016**, *7*, 13300.

(29) Liu, T.-F.; Zou, L.; Feng, D.; Chen, Y.-P.; Fordham, S.; Wang, X.; Liu, Y.; Zhou, H.-C. Stepwise synthesis of robust metal-organic frameworks via postsynthetic metathesis and oxidation of metal nodes in a single-crystal to single-crystal transformation. *J. Am. Chem. Soc.* **2014**, *136*, 7813−7816.

(30) Wang, J.-H.; Zhang, Y.; Li, M.; Yan, S.; Li, D.; Zhang, X.-M. Solvent-assisted metal metathesis: a highly efficient and versatile route towards synthetically demanding chromium metal-organic frameworks. *Angew. Chem., Int. Ed.* **2017**, *56*, 6478−6482.

(31) Rostami, J.; Benselfelt, T.; Maddalena, L.; Avci, C.; Sellman, F. A.; Cinar Ciftci, G.; Larsson, P. A.; Carosio, F.; Akhtar, F.; Tian, W.; Wågberg, L. Shaping 90 wt% nanoMOFs into robust multifunctional aerogels using tailored bio-based nanofibrils. *Adv. Mater.* **2022**, *34*, 2204800.

(32) Ding, N.; Li, H.; Feng, X.; Wang, Q.; Wang, S.; Ma, L.; Zhou, J.; Wang, B. Partitioning MOF-5 into confined and hydrophobic compartments for carbon capture under humid conditions. *J. Am. Chem. Soc.* **2016**, *138*, 10100−10103.

(33) Rao, K. P.; Higuchi, M.; Sumida, K.; Furukawa, S.; Duan, J.; Kitagawa, S. Design of superhydrophobic porous coordination polymers through the introduction of external surface corrugation by the use of an aromatic hydrocarbon building unit. *Angew. Chem., Int. Ed.* **2014**, *53*, 8225−8230.

(34) Feng, L.; Wang, Y.; Zhang, K.; Wang, K.-Y.; Fan, W.; Wang, X.; Powell, J. A.; Guo, B.; Dai, F.; Zhang, L.; Wang, R.; Sun, D.; Zhou, H.-C. Molecular pivot-hinge installation to evolve topology in rare-earth metal-organic frameworks. *Angew. Chem., Int. Ed.* **2019**, *58*, 16682−16690.

(35) Lv, X.-L.; Feng, L.; Xie, L.-H.; He, T.; Wu, W.; Wang, K.-Y.; Si, G.; Wang, B.; Li, J.-R.; Zhou, H.-C. Linker desymmetrization: Access to a series of rare-earth tetracarboxylate frameworks with eight-connected hexanuclear nodes. *J. Am. Chem. Soc.* **2021**, *143*, 2784−2791.

(36) Gao, Y.; Zhang, M.; Chen, C.; Zhang, Y.; Gu, Y.; Wang, Q.; Zhang, W.; Pan, Y.; Ma, J.; Bai, J. A low symmetry cluster meets a low symmetry ligand to sharply boost MOF thermal stability. *Chem. Commun.* **2020**, *56*, 11985−11988.

https://doi.org/10.1021/jacs.3c00957
J. Am. Chem. Soc. 2023, 145, 9665−9671

(37) Gao, W.-Y.; Chrzanowski, M.; Ma, S. Metal-metalloporphyrin frameworks: a resurging class of functional materials. *Chem. Soc. Rev.* **2014**, *43*, 5841−5866.
(38) Zhao, M.; Ou, S.; Wu, C.-D. Porous metal-organic frameworks for heterogeneous biomimetic catalysis. *Acc. Chem. Res.* **2014**, *47*, 1199−1207.
(39) Zhang, X.; Wasson, M. C.; Shayan, M.; Berdichevsky, E. K.; Ricardo-Noordberg, J.; Singh, Z.; Papazyan, E. K.; Castro, A. J.; Marino, P.; Ajoyan, Z.; Chen, Z.; Islamoglu, T.; Howarth, A. J.; Liu, Y.; Majewski, M. B.; Katz, M. J.; Mondloch, J. E.; Farha, O. K. A historical perspective on porphyrin-based metal-organic frameworks and their applications. *Coord. Chem. Rev.* **2021**, *429*, No. 213615.
(40) Fang, Z.-B.; Liu, T.-T.; Liu, J.; Jin, S.; Wu, X.-P.; Gong, X.-Q.; Wang, K.; Yin, Q.; Liu, T.-F.; Cao, R.; Zhou, H.-C. Boosting interfacial charge-transfer kinetics for efficient overall CO_2 photoreduction via rational design of coordination spheres on metal-organic frameworks. *J. Am. Chem. Soc.* **2020**, *142*, 12515−12523.
(41) Yang, L.; Cai, P.; Zhang, L.; Xu, X.; Yakovenko, A. A.; Wang, Q.; Pang, J.; Yuan, S.; Zou, X.; Huang, N.; Huang, Z.; Zhou, H.-C. Ligand-directed conformational control over porphyrinic zirconium metal-organic frameworks for size-selective catalysis. *J. Am. Chem. Soc.* **2021**, *143*, 12129−12137.
(42) Wang, K.; Feng, D.; Liu, T.-F.; Su, J.; Yuan, S.; Chen, Y.-P.; Bosch, M.; Zou, X.; Zhou, H.-C. A series of highly stable mesoporous metalloporphyrin Fe-MOFs. *J. Am. Chem. Soc.* **2014**, *136*, 13983−13986.
(43) Liu, Q.; Cong, H.; Deng, H. Deciphering the spatial arrangement of metals and correlation to reactivity in multivariate metal-organic frameworks. *J. Am. Chem. Soc.* **2016**, *138*, 13822−13825.
(44) Muniappan, S.; Lipstman, S.; George, S.; Goldberg, I. Porphyrin framework solids. synthesis and structure of hybrid coordination polymers of tetra(carboxyphenyl)porphyrins and lanthanide-bridging ions. *Inorg. Chem.* **2007**, *46*, 5544−5554.
(45) Feng, D.; Wang, K.; Wei, Z.; Chen, Y.-P.; Simon, C. M.; Arvapally, R. K.; Martin, R. L.; Bosch, M.; Liu, T.-F.; Fordham, S.; Yuan, D.; Omary, M. A.; Haranczyk, M.; Smit, B.; Zhou, H.-C. Kinetically tuned dimensional augmentation as a versatile synthetic route towards robust metal-organic frameworks. *Nat. Commun.* **2014**, *5*, 5723.
(46) Feng, D.; Liu, T.-F.; Su, J.; Bosch, M.; Wei, Z.; Wan, W.; Yuan, D.; Chen, Y.-P.; Wang, X.; Wang, K.; Lian, X.; Gu, Z.-Y.; Park, J.; Zou, X.; Zhou, H.-C. Stable metal-organic frameworks containing single-molecule traps for enzyme encapsulation. *Nat. Commun.* **2015**, *6*, 5979.
(47) Liu, G.; Cui, H.; Wang, S.; Zhang, L.; Su, C.-Y. A series of highly stable porphyrinic metal-organic frameworks based on iron-oxo chain clusters: design, synthesis and biomimetic catalysis. *J. Mater. Chem. A* **2020**, *8*, 8376−8382.
(48) Verma, G.; Kumar, S.; Vardhan, H.; Ren, J.; Niu, Z.; Pham, T.; Wojtas, L.; Butikofer, S.; Echeverria Garcia, J. C.; Chen, Y.-S.; Space, B.; Ma, S. A robust soc-MOF platform exhibiting high gravimetric uptake and volumetric deliverable capacity for on-board methane storage. *Nano Res.* **2021**, *14*, 512−517.
(49) Vallés-García, C.; Gkaniatsou, E.; Santiago-Portillo, A.; Giménez-Marqués, M.; Álvaro, M.; Greneche, J.-M.; Steunou, N.; Sicard, C.; Navalón, S.; Serre, C.; García, H. Design of stable mixed-metal MIL-101(Cr/Fe) materials with enhanced catalytic activity for the Prins reaction. *J. Mater. Chem. A* **2020**, *8*, 17002−17011.
(50) Aguirre-Díaz, L. M.; Reinares-Fisac, D.; Iglesias, M.; Gutiérrez-Puebla, E.; Géndara, F.; Snejko, N.; Monge, M. Á. Group 13th metal-organic frameworks and their role in heterogeneous catalysis. *Coord. Chem. Rev.* **2017**, *335*, 1−27.
(51) Li, Y.-L.; Alexandrov, E. V.; Yin, Q.; Li, L.; Fang, Z.-B.; Yuan, W.; Proserpio, D. M.; Liu, T.-F. Record complexity in the polycatenation of three porous hydrogen-bonded organic frameworks with stepwise adsorption behaviors. *J. Am. Chem. Soc.* **2020**, *142*, 7218−7224.
(52) Wu, Q.-J.; Liang, J.; Huang, Y.-B.; Cao, R. Thermo-, electro-, and photocatalytic CO_2 conversion to value-added products over porous metal/covalent organic frameworks. *Acc. Chem. Res.* **2022**, *55*, 2978−2997.
(53) Ding, M.; Jiang, H.-L. Incorporation of imidazolium-based poly(ionic liquid)s into a metal-organic framework for CO_2 capture and conversion. *ACS Catal.* **2018**, *8*, 3194−3201.
(54) Pal, T. K.; De, D.; Bharadwaj, P. K. Metal-organic frameworks for the chemical fixation of CO_2 into cyclic carbonates. *Coord. Chem. Rev.* **2020**, *408*, No. 213173.
(55) Le, D. H.; Loughan, R. P.; Gładysiak, A.; Rampal, N.; Brooks, I. A.; Park, A.-H. A.; Fairen-Jimenez, D.; Stylianou, K. C. Lanthanide metal-organic frameworks for the fixation of CO_2 under aqueous-rich and mixed-gas conditions. *J. Mater. Chem. A* **2022**, *10*, 1442−1450.
(56) Wang, Y.; Shi, T.; Fan, Q.-Y.; Liu, Y.; Zhang, A.; Li, Z.; Hao, Y.; Chen, L.; Liu, F.; Gu, X.; Zeng, S. Discovering surface structure and the mechanism of graphene oxide-triggered CeO_2-WO_3/TiO_2 catalysts for NO abatement with NH_3. *ACS Catal.* **2022**, *12*, 8386−8403.
(57) Wang, B.; Wang, M.; Han, L.; Hou, Y.; Bao, W.; Zhang, C.; Feng, G.; Chang, L.; Huang, Z.; Wang, J. Improved activity and SO_2 resistance by Sm-modulated redox of $MnCeSmTiO_x$ mesoporous amorphous oxides for low-temperature NH_3-SCR of NO. *ACS Catal.* **2020**, *10*, 9034−9045.
(58) Sheldrick, G. M. *SHELXS-97, Programs for X-ray crystal structure solution*; University of Göttingen: Germany, 1997.
(59) Dolomanov, O. V.; Bourhis, L. J.; Gildea, R. J.; Howard, J. A. K.; Puschmann, H. OLEX2: a complete structure solution, refinement and analysis program. *J. Appl. Crystallogr.* **2009**, *42*, 339−341.
(60) Spek, A. L. Single-crystal structure validation with the program PLATON. *J. Appl. Crystallogr.* **2003**, *36*, 7−13.

Recommended by ACS

Blending Aryl Ketone in Covalent Organic Frameworks to Promote Photoinduced Electron Transfer
Mingjie Liu, Zhiguo Zhang, *et al.*
APRIL 17, 2023
JOURNAL OF THE AMERICAN CHEMICAL SOCIETY
READ

Ingenious Artificial Leaf Based on Covalent Organic Framework Membranes for Boosting CO_2 Photoreduction
Shuaiqi Gao, Jianji Wang, *et al.*
APRIL 19, 2023
JOURNAL OF THE AMERICAN CHEMICAL SOCIETY
READ

Three-Component Donor−π−Acceptor Covalent−Organic Frameworks for Boosting Photocatalytic Hydrogen Evolution
Ziping Li, Xiaoming Liu, *et al.*
MARCH 14, 2023
JOURNAL OF THE AMERICAN CHEMICAL SOCIETY
READ

Topological Isomerism in Three-Dimensional Covalent Organic Frameworks
Yaozu Liu, Qianrong Fang, *et al.*
APRIL 18, 2023
JOURNAL OF THE AMERICAN CHEMICAL SOCIETY
READ

Get More Suggestions >

https://doi.org/10.1021/jacs.3c00957
J. Am. Chem. Soc. 2023, 145, 9665−9671